Ultrahigh Densities and Volume Recombination inside the Separatrix of the Alcator C-Mod Tokamak

B. Lipschultz, J. L. Terry, C. Boswell, A. Hubbard, B. LaBombard, and D. A. Pappas
Massachusetts Institute of Technology Plasma Science and Fusion Center, Cambridge, Massachusetts 02139
(Received 7 May 1998)

MARFEs are experimentally studied using spectroscopic techniques to determine their internal characteristics. We find the local density and temperature in the MARFE to be $(2-3) \times 10^{21}$ m^{-3} and 0.7–1.0 eV, respectively. The volume recombination rate is also large in the MARFE, $(5-10) \times 10^{22}$ s^{-1}, similar in magnitude to the plasma source rate in the core. Because this plasma sink is located in confined regions of the plasma, the MARFE acts like a limiter; ions "recycle" from the MARFE as neutrals. These characteristics have not been predicted by current models. [S0031-9007(98)06712-X]

PACS numbers: 52.55.Fa, 34.80.Lx, 52.25.Qt, 52.25.Rv

MARFEs are quasi-steady-state tokamak phenomena characterized by the appearance of a toroidally symmetric band of intense radiation which forms at the inside edge (major radius) of tokamak plasmas (see Ref. [1] and references therein). MARFEs can strongly affect the core by modifying fueling and impurity sources. It has been found that MARFEs typically occur at a fraction, 50%–90%, of the density limit [2,3]. The poloidal location of the MARFE at the high-field edge and its radial extent reaching to closed flux surfaces have been seen as evidence for poloidally asymmetric transport of power across flux surfaces in the core plasma [1,4]. All of the above characteristics have led to the study of MARFEs both experimentally [1–3,5–9] and theoretically [10–18]. The modeling of the MARFE as an impurity radiation-condensation instability is fairly well accepted. Local radiation losses compete with parallel and perpendicular heat conduction to determine an equilibrium density and temperature. The characteristics of MARFEs thus have much in common with models of solar prominences [12,19].

In this Letter we present experimentally determined MARFE characteristics, including direct measurements of higher density, $n_e \sim (2-3) \times 10^{21}$ m^{-3} and lower temperature, $T_e \sim 0.7$ eV than previously inferred. A surprising new finding is that 3-body recombination is occurring in the MARFE at a high rate ($\leq 10^{23}$ s^{-1}), enough to neutralize most of the plasma outflow from the core plasma. Such a significant plasma sink has not been previously predicted.

The measurements presented here are from the Alcator C-Mod tokamak. Basic characteristics of the experiment and diagnostics are described elsewhere [20]. The data used in this study were acquired with 5.3 tesla toroidal field at the plasma center and plasma currents in the range 0.8–1.0 MA. Both diverted and limited discharges were used in these studies. The results were essentially the same in these two cases. Differences will be noted where applicable.

The most important diagnostics used for this study were two spectrometers, one each to measure the Balmer and Lyman series spectra, and a diode array filtered for D_α.

The general characteristics of the MARFE are shown in Fig. 1. The plasma equilibrium is changed from limited to diverted at 0.26 s and remains so for the remainder of the discharge. The MARFE period (0.14 to 0.5 s) is exemplified by C-II emission from the inner wall 1(d). When the MARFE ends the core plasma radiation drops

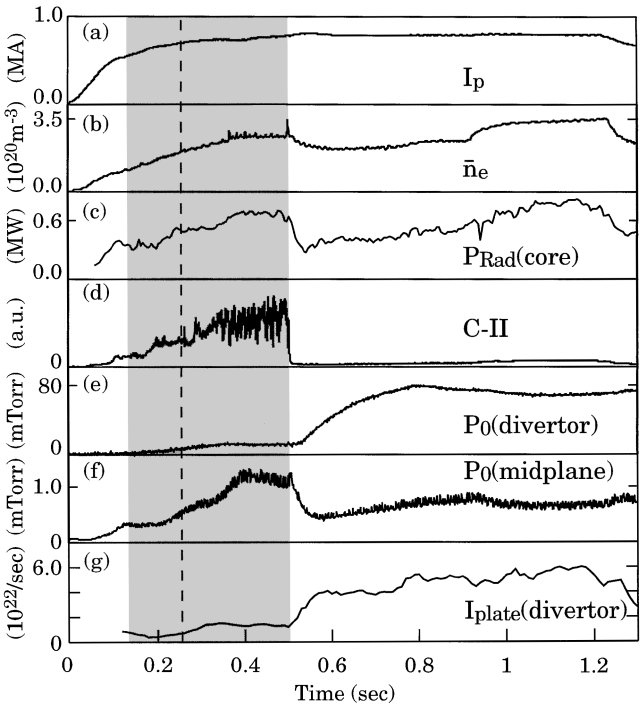

FIG. 1. An example of a MARFE occurrence. The MARFE (shaded region of time) starts at 0.14 s. The plasma is diverted from 0.26 s (vertical dashed line) onward. (a) Plasma current, (b) line-averaged density through the core plasma, (c) radiation from the core, (d) C-II emission from the MARFE region, (e) D_2 pressure in the divertor region, (f) D_2 pressure outside the divertor region at the midplane, and (g) ion current to the divertor plates.

1(c) and recycling increases in the divertor: There is a large increase in ion current to the divertor plates 1(g), the divertor pressure rises 1(e), and the midplane pressure, outside the divertor, drops 1(f).

A charge-coupled device (CCD) camera, filtered for D_α, has been used to deduce the MARFE location and size. In Fig. 2(a) we show a contour plot of brightness from the part of the CCD image where the view is tangent to the inner wall and the MARFE (diverted discharge). The peak in MARFE emission is located 2–3 cm radially out from the inner wall (shaded region) and inside the separatrix (division between closed flux surfaces in the core and open flux surfaces in the edge, indicated by the dashed line). The vertical profile of the emission through the MARFE's radial center is shown in Fig. 2(b). From this information we find the vertical and radial FWHM of the MARFE D_α emission to be approximately 13 cm and 2 cm, respectively. The vertical location of the MARFE does vary over time but generally stays in the region $-10 \le z \le 10$ cm. For limited plasmas the vertical FWHM is $\sim$10 cm and the center tends to be lower, ~ -5 cm. These minor differences between limited and divertor plasma MARFEs may not be statistically significant in that we have not captured a large number of these events ($\sim$10) with the CCD camera.

We have analyzed emission from the Balmer and Lyman series spectra and nearby continuum to determine more of the MARFE characteristics. A typical Balmer spectrum (instrumental resolution 0.15–0.2 nm) from a horizontal view which encompasses the entire vertical extent of the MARFE is shown in Fig. 3(a). The Lyman spectrum (instrumental resolution 0.15 nm) from a 1.5 cm vertical section of the MARFE is shown in Fig. 3(b). The intensities would decrease much more strongly as a function of increasing upper transition level p if the population were dominated by excitation from the ground state [21]. These spectra show that the populations of the excited states are dominated by recombination. Note that the lines in the Balmer spectrum are significantly broadened compared to the instrumental width. We fit a Voigt profile to these line shapes to obtain the FWHM of the $p = 6, 7, 8, 9 \rightarrow 2$ Balmer series lines. [An example is shown in Fig. 4(a).] Using standard Stark analysis techniques (e.g., Ref. [22]), we find that the density in the MARFE is $(2.2 \pm 0.3) \times 10^{21}$ m^{-3} from these lines. Similar analyses applied to a number of MARFEs result in densities in the range $(2-3) \times 10^{21}$ m^{-3}.

In such recombination-dominated spectra the population density for each level should scale according to the Saha-Boltzmann distribution. We perform a least-squares fit of the population densities to obtain T_e:

$$n_p \propto \frac{p^2}{T_e^{3/2}} \exp\left(\frac{13.605}{T_e p^2}\right), \tag{1}$$

where $(13.605/p^2)$ is the ionization energy for the pth level. The fit, shown in Fig. 4(b) as a dashed line, yields a local T_e of 1.0 ± 0.2 eV. Because of the overlap of the $p = 9$ and $10 \rightarrow 2$ lines as well as their large "wings," which are difficult to fit, we have only included the $p = 5$ through $8 \rightarrow 2$ lines in this T_e analysis. For illustration of the dependence of the fit on T_e, we also show the relative Saha population densities for $T_e = 0.6$ eV (normalized to $p = 6$) which do not fit the data. The uncertainty in T_e is based on the estimated effect of plasma opacity to the Lyman series lines on the population distribution as well

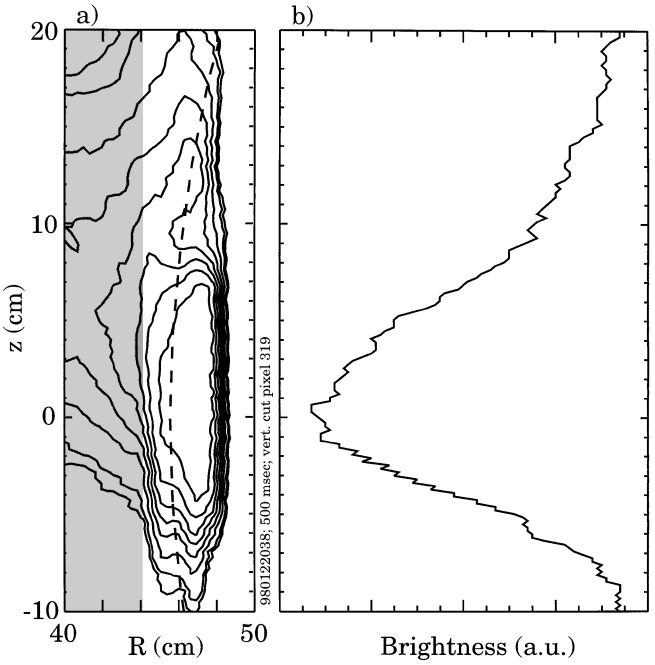

FIG. 2. Data from a CCD camera tangential view of the MARFE region. The camera is located below the midplane ($z = 0$). Light is filtered to pass only D_α: (a) contour plot of the tangential view. The dashed line corresponds to the plasma separatrix. The shaded area is the wall. Contours trailing off to smaller major radius show the toroidal nature of the MARFE. (b) A vertical cut through the data of (a).

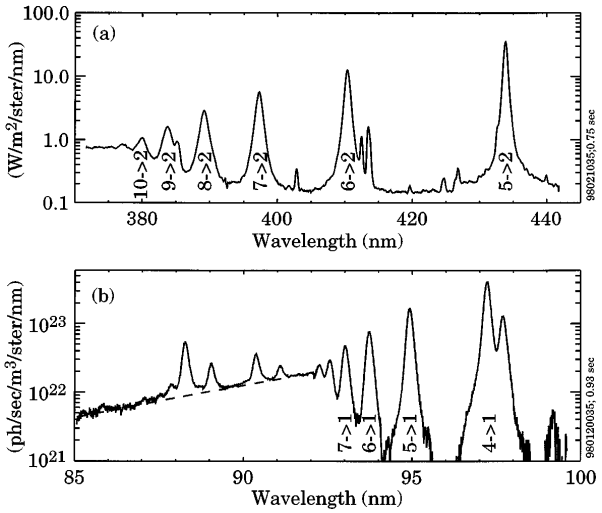

FIG. 3. D^0 spectrum from the MARFE in the visible (a) and VUV (b). Dashed line in (b) represents a radiative recombination model assuming a viewing path length of 1.5 cm, $n_e \sim 1.8 \times 10^{21}$ m^{-3} and $T_e = 0.7$ eV.

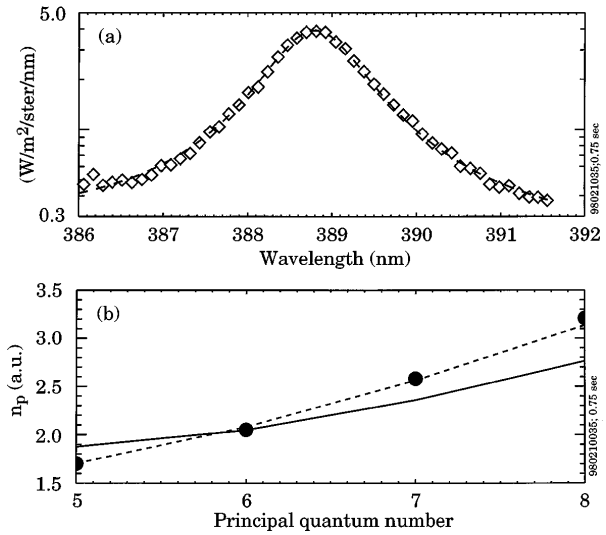

FIG. 4. Analysis of the Balmer spectrum. (a) Voigt fit (———) to the $p = 8 \rightarrow 2$ intensity ($\diamond$) of Fig. 3(a). Stark analysis yields $n_e \sim 2.2 \times 10^{21}$ m^{-3}. (b) Least squares fit (– – – –) of Saha-Boltzmann distribution to population densities (●) yields $T_e \sim 1.0$ eV. The relative distribution normalized to $p = 6 \rightarrow 2$ for $T_e = 0.6$ eV is shown as well (———).

as possible excitation from the ground state. Variations in inferred T_e are found from one MARFE occurrence to another, or even during a MARFE (0.8–1.25 eV).

As an independent confirmation of the density and temperatures determined above, we have modeled the vacuum ultraviolet (VUV) spectrum near the Lyman series limit [Fig. 3(b)]. The continuum intensity for $\lambda \leq 91$ nm is dominated by free-bound radiative recombination and is $\propto n_e^2 \Delta L e^{-h\nu/kT}$, where ΔL is the radial width of the emission region. Using ΔL from the CCD image the data are well-matched by $n_e = (1.9 \pm 0.4) \times 10^{21}$ m^{-3} and $T_e = 0.7 \pm 0.1$ eV. We believe the determination of T_e by this method to be more accurate than from line intensities because it mirrors the electron distribution function.

The density in the MARFE is $\geq$5 times the highest previously measured in a MARFE [1] or obtained from modeling [14]. The temperature is lower. In the absence of a MARFE, this region just inside the separatrix is typically characterized by $n_e \sim 10^{20}$ m^{-3}, $T_e \sim 70$–100 eV, and much less D_α emission. The peak density and temperature in the center of this plasma ($R = 67.5$ cm) were 2.5×10^{20} m^{-3} and 1200 eV, respectively.

If the MARFE plasma is opaque to Lyman series radiation, the local recombination and ionization rates are strongly affected. By measuring Ly$_\beta$ and D_α intensities along the same line-of-sight through the MARFE, we find that up to 50% of the Ly$_\beta$ photons are trapped and lost in the MARFE region, which implies even stronger trapping ($\geq$95%) of Ly$_\alpha$ emission. We have quantified the effect of Ly$_{\alpha,\beta}$ trapping on the recombination rate by modeling the photon transport through the recombination region as purely diffusive (in space only). The modeling [21] shows that at these levels of trapping the recombination rate is reduced by a factor ~5.

Based on the above information we have estimated the volume recombination rate in the MARFE. The primary method used in this analysis is based on previous work (Ref. [21], and references therein), in which a formalism is employed which allows one to determine the recombination rate, given knowledge of the emitting region n_e, T_e, D^0 line brightness, and opacity to the Lyman series. We have applied this formalism to the emission lines of D_α (diode array) and D_γ (visible spectrometer) using the MARFE characteristics discussed above. The resultant total recombination rate, S_{recomb}, is in the range $(5–10) \times 10^{22}$ s^{-1}. The radiative cost per recombination (ionization) ~10 eV (20 eV). The MARFE D^0 radiation should be $\sim S_{\text{recomb}} \times (30 \text{ eV}) \sim 240–480$ kW. The *measured* D^0 radiative losses are in agreement; 150–300 kW. It is important to note that from the CCD image we know that *recombination is occurring on closed flux surfaces (core plasma).*

The MARFE is a significant sink for ions. In similar plasmas to that shown in Figs. 1–4, but without MARFEs present, the total ion source rate outside the divertor has been measured to be in the range $(1–8) \times 10^{22}$ s^{-1} [23]. A fraction ($\leq$50%) of this source is inside the separatrix. This provides us with a rough measure of the radial plasma flow in the core because, in steady state, ion sources and sinks must be balanced. So the MARFE ion sink due to recombination is similar in magnitude to the ion source for the core.

Further evidence of the MARFE's ion sink action is found in the evolution of the ion current (a measure of electron flow as well) to the outer divertor plate [Fig. 1(g)]. After the MARFE ends, the ion current to the divertor plates increases rapidly by an amount similar to the MARFE recombination sink. The implication is that a significant fraction of the core radial plasma flux recombines in the MARFE before crossing the separatrix and traveling to the outer divertor. The location of the recombination, as indicated by the D_α emission in the CCD image (Fig. 2), indicates this to be true as well. The MARFE acts effectively like a toroidal limiter extending inside the separatrix. Plasma recycles from it; ions and electrons enter the MARFE "limiter" and return to the core as neutrals. This flow pattern is qualitatively similar to the ion flow pattern found in modeling [14]. However, the perpendicular flows would likely have a stronger neutral component in this case.

We can estimate the ion flow velocity in the MARFE based on the above ion sink rate. The poloidal component of the ion velocity, v_{pol}, is given by the following:

$$2 n_e v_{\text{pol}} A_{\text{pol}} \sim S_{\text{recomb}} , \qquad (2)$$

where A_{pol} is the poloidal area of the MARFE ($= 2\pi R_{\text{MARFE}} \Delta R_{\text{MARFE}}$). Given the local magnetic field, we obtain the parallel velocity, $v_\parallel \sim (2–4) \times 10^3$ m/s and a Mach number in the range 0.3–0.6 (assuming $T_e = 1$ eV). The corresponding convected power ($= 5 T_e \times S_{\text{recomb}}$) in the MARFE is 40–80 kW,

a significant fraction of the D^0 radiated power. These characteristics are again limiter-like because at the surface of a limiter the Mach number ≥ 1 and the power flow is convective.

The location of the MARFE inside the separatrix affects other aspects of the core plasma. Measurements of n_e and T_e on the same flux surface, but away from the MARFE were made using electron cyclotron emission (T_e) and density interferometry techniques [20]. T_e in this region is lower during the MARFE ($\sim 25-65$ eV) than without (95 eV). To within experimental resolution n_e does not vary. These results point to large poloidal asymmetries in density and temperature inside the separatrix. Given the MARFE's characteristics (n_e and T_e, trapping of $\mathrm{Ly}_{\alpha,\beta}$), the neutral density *inside* the MARFE could be of the same order as n_e there. The presence of high neutral densities could lead to plasma pressure variation (ion momentum loss) in the MARFE and thus on closed flux surfaces as well.

Characteristics of a divertor phenomenon termed "divertor detachment" [e.g., Ref. 24] are similar to that of MARFEs in C-Mod. When divertor detachment occurs in C-Mod, a toroidal band of D^0 radiation appears in the plasma between the x-point and either or both divertor plates [21,25]. The emission spectrum is dominated by recombination; $n_e = 1-1.5 \times 10^{21}\ \mathrm{m}^{-3}$ and $T_e \leq 1$ eV. The recombination rate in this region is less than that in the MARFE ($\leq 8 \times 10^{21}\ \mathrm{s}^{-1}$) simultaneous with large reductions in ion currents to the divertor plates and little effect on the core plasma.

If the density is increased further following formation of a MARFE, a poloidally detached plasma often occurs. In these cases the core plasma is enveloped, toroidally and poloidally by a radiating surface, at or inside the last closed flux surface or separatrix [26–28]. There is little or no plasma flow to the surrounding walls, leading us to speculate that recombination may be the plasma sink. Preliminary spectral measurements from C-Mod, for the brief periods during which poloidally detached plasmas appear, are consistent with this hypothesis.

The results in this paper are consistent with the basic understanding of the MARFE. The existing models appear correct in assuming a radiation-condensation instability allowing for both hydrogen and impurity excitation energy sinks. However, recombination is not included in any model except Ref. [14], and the local density has not been increased to that of Alcator C-Mod [$(1-2) \times 10^{20}\ \mathrm{m}^{-3}$ without a MARFE]. These are probable reasons for the C-Mod MARFE characteristics not being predicted. Volume recombination radiation provides the energy sink at low T_e where impurities cannot. In order to be able to reproduce the other limiterlike characteristics seen in C-Mod, such as significant perpendicular flow of neutrals and high Mach number ion flows, it may be important to include other processes such as neutral-neutral and ion-neutral collisions.

In summary we have shown that n_e and T_e in the MARFE are significantly different from that found in previous studies. The presence of recombination as a strong plasma sink is potentially important. The presence of such a perturbation inside the plasma core has implications for core transport and, in particular, neutral and ion flows. These MARFE characteristics show that the current models of a MARFE are incomplete. The existence of recombining, high-density MARFEs in other tokamaks awaits further measurements.

The authors wish to thank Dr. S. I. Krasheninnikov as well as Professors I. H. Hutchinson and P. C. Stangeby for extremely helpful discussions regarding MARFEs. The work reported here was supported by the U.S. Department of Energy under Contract No. DE-AC02-78ET51013.

[1] B. Lipschultz, J. Nucl. Mater. **145–147**, 15 (1986).
[2] B. Lipschultz *et al.*, Nucl. Fusion **24**, 977 (1984).
[3] G. Stabler *et al.*, Nucl. Fusion **32**, 1557 (1992).
[4] The ASDEX Team, Max Planck Institut für Plasmaphysik, Garching, IPP III/73, 1973.
[5] H. Niedermeyer *et al.*, Max-Planck-Institut für Plasmaphysik Report No. IPP III/90, 1983.
[6] D. R. Baker *et al.*, Nucl. Fusion **22**, 807 (1982).
[7] F. Alladio *et al.*, Phys. Lett. **90A**, 405 (1982).
[8] F. P. Boody *et al.*, J. Nucl. Mater. **145–147**, 196 (1987).
[9] T. Nishitani *et al.*, J. Nucl. Mater. **176 & 177**, 763 (1990).
[10] T. Stringer, Joint European Torus Report No. JET-DN-T(85)8, 1985 (unpublished).
[11] J. Neuhauser, W. Schneider, and R. Wunderlich, Nucl. Fusion **26**, 1679 (1986).
[12] J. F. Drake, Phys. Fluids **30**, 2429 (1987).
[13] J. Kesner and J. P. Freidberg, Nucl. Fusion **35**, 115 (1995).
[14] H. Kastelewicz, R. Schneider, and J. Neuhauser, Plasma Phys. Control. Fusion **37**, 723 (1995).
[15] A. DePloey *et al.*, Plasma Phys. Controlled Fusion **39**, 423 (1997).
[16] W. M. Stacey, Phys. Plasmas **3**, 2673 (1996).
[17] D. Kh. Morozov and J. J. E. Herrera, Plasma Phys. Controlled Fusion **37**, 285 (1995).
[18] B. Meerson, Rev. Mod. Phys. **68**, 215 (1996).
[19] G. B. Field, Astrophys. J. **142**, 531 (1965).
[20] I. H. Hutchinson *et al.*, Phys. Plasmas **1**, 1511 (1994).
[21] J. L. Terry *et al.*, Phys. Plasmas **5**, 1759 (1998).
[22] R. D. Bengston, J. D. Tannich, and P. Kepple, Phys. Rev. A **1**, 532 (1970).
[23] C. Kurz *et al.*, Plasma Phys Controlled Fusion **39**, 963 (1997).
[24] C. S. Pitcher and P. C. Stangeby, Plasma Phys. Controlled Fusion **39**, 779 (1997).
[25] M. Fenstermacher *et al.*, Phys. Plasmas **4**, 1761 (1997).
[26] G. M. McCracken *et al.*, J. Nucl. Mater. **145–147**, 181 (1987).
[27] U. Samm *et al.*, KFA Jul-Report No. 2123 (1987).
[28] J. D. Strachan *et al.*, J. Nucl. Mater. **145–147**, 186 (1987).